

# Comparison of grain-size distributions between nearshore sections and a deep-water sediment core from Dali Lake, North China, and inferred Holocene lake-level changes

Jin Liu · Yong Wang · Tingdong Li · Fei Tian ·  
Jingsong Yang

Received: 8 April 2015 / Accepted: 20 June 2016 / Published online: 1 July 2016  
© Springer Science+Business Media Dordrecht 2016

**Abstract** The grain-size distribution of the sediments of closed lake basins is sensitive to lake-level changes and thus to changes in regional climate. Deep-water areas of lakes potentially yield high resolution, continuous records of sedimentation and lake-level changes. In contrast, the marginal areas of lake basins accumulate sediment in a wave-dominated, high-energy environment and may be more sensitive to lake-level changes than deep-water environments, but they might also be more affected by sedimentary hiatuses. Here, we present grain-size data from two sections of exposed nearshore sediments of Dali Lake, North China, and compare them with previously published results from a sediment core from the lake center. We used the grain size-standard deviation method to distinguish various grains-size components of the nearshore sediments, and compared the results with those from surface sediments from various depths in order to investigate past lake-level changes. Combining the grain-size results with a radiocarbon

chronology, we defined four lake-level stages during the Holocene: (1) An intermediate lake level from early Holocene to 10.0 cal ka BP. (2) A high lake level from 10.0 to 6.6 cal ka BP. (3) A decline to an intermediate lake level from 6.6 to 1.0 cal ka BP. (4) An abrupt fall to a low lake level from 1.0 cal ka BP to the present when the marginal section was covered with eolian sand. Our results indicate that the total amplitude of lake-level variation during the Holocene was greater than 45 m. This record of lake-level change is in good agreement with previous results obtained from the lake center, and it indicates that the grain-size standard deviation method may be well suited for lake-level reconstruction from nearshore sediments. Moreover, the marginal sections provide evidence of an abrupt short-lived lake-level decline more clearly than the deep-water core.

**Keywords** Grain-size component · Standard deviation · Lake-level · Holocene · Dali Lake · East Asian Summer Monsoon

---

J. Liu · Y. Wang (✉) · T. Li · F. Tian  
Institute of Geology, Chinese Academy of Geological  
Sciences, Beijing 100037, China  
e-mail: wangyong@cags.ac.cn

J. Liu  
China University of Geosciences, Beijing 100083, China

J. Yang  
Institute of Hydrogeology and Environmental Geology,  
Chinese Academy of Geological Sciences,  
Shijiazhuang 250013, China

## Introduction

Previous studies in the northern margin of East Asian Summer Monsoon (EASM) region have used hydrologic and climatic records from sediment cores from the extant lakes and inferred a cold and dry climate in the early and late Holocene, and a humid environment

in the mid Holocene (Xiao et al. 2004; Wen et al. 2010). The sediments from a deep lake can be assumed to have accumulated continuously and to provide a high resolution record of environmental change, whereas nearshore sediments provide a direct record of high lake-level stands, as well as information about geological events and absolute changes in lake size (Cohen 2003; Reheis et al. 2014). The rate of lake-level change can be estimated given adequate chronological control (Nishizawa et al. 2013). In summary, in order to reconstruct regional hydrological changes reliably, it is necessary to synthesize both the nearshore and offshore sedimentary records of the lake basin (Bacon et al. 2006; Negrini et al. 2006; Reheis et al. 2012; Benson et al. 2013; Reheis et al. 2014).

Grain-size time series have been used widely to study monsoonal evolution in the boundary of the EASM region (Peng et al. 2005; Zhang et al. 2012). The grain-size distribution of lacustrine sediments provides important information about the depositional environment, hydrodynamics, and changes in lake level and regional climate (Håkanson and Jansson 1983; Campbell 1998; Xiao et al. 2009, 2015). The frequency plot of a single sedimentary component, or of a sample generated by a single sediment transport process, exhibits a smooth unimodal distribution curve, while the presence of two or more sedimentary components or transport sources results in bimodal or multimodal frequency distribution curves (Krumbein 1938; Folk and Ward 1957; Visher 1969; Ashley 1978). In the case of the polymodal grain-size distribution curves of bulk samples, common descriptive statistical parameters such as the mean grain size, skewness and standard deviation of bulk samples cannot be reliable indicators of the sedimentary environment. Therefore, the partitioning of each sedimentary component and relating it to a specific source or transportation process is commonly employed. Traditional graphical techniques are considered to be subjective and imprecise for accurately partitioning grain-size distributions (Middleton 1976; Ashley 1978). Increasingly, mathematical methods are used for the purpose: e.g. the grain size-standard deviation method (Boulay et al. 2003; Ma et al. 2013), the lognormal distribution function method (Qin et al. 2005; Xiao et al. 2009), the Weibull function method (Sun et al. 2002),

EMMA (end-member-modelling algorithm) analysis (Weltje 1997; Liu et al. 2009), and primary component analysis (Wang et al. 2014).

Dali Lake in North China has developed a sequence of lake terraces since the later part of the Late Pleistocene, which demonstrates that the area has experienced large-amplitude climatic fluctuations (Li et al. 1990). Xiao et al. (2008, 2009) and Liu et al. (2015) presented the results of grain size, total organic and inorganic carbon and biomagnetic records in a sediment core from the central part of Dali Lake, and reconstructed the history of lake-level change since 11.5 cal ka BP (thousands of calibrated years before Present). In the present paper, we focus on the grain-size distribution record of two nearshore sections and compare the finding with previous results from the central part of the lake.

#### Study area

Dali Lake (43°13′–43°23′N, 116°23′–116°58′E; elevation 1226 m a.s.l.) is a closed lake basin located in the East Asian Summer Monsoon transition area (Fig. 1, the background is downloaded from <http://gdem.ersdac.jpacesystems.or.jp/index.jsp>, ASTER GDEM is a product of METI and NASA). The surface area was 188.48 km<sup>2</sup> in 2010 (Zhen et al. 2013) and the maximum water depth is 11 m. The lake is ice-covered from the end of November until April. Two small lakes (Ganggeng Nor and Duolun Nor, with respective areas of 17.8 and 2.0 km<sup>2</sup>) are situated to the east and west of Dali Lake along the Xilamulun Fault (Geng and Zhang 1988) (Fig. 1). Two permanent rivers enter the eastern and northeastern parts of the lake basin, and two seasonal streams enter the western part. The total discharge of the four rivers was about  $4424.49 \times 10^4$  m<sup>3</sup> in 2012 (Zhen et al. 2014). In the lake catchment, exposed rocks are mainly Cenozoic basalt in the north and west (Geng and Zhang 1988), while eolian sand and ancient lacustrine sediments (covered with eolian sand) are distributed in the south and east. Tectonic activity in the upstream of Xilamulun River was stable in early and middle Holocene and became more active in the late Holocene (2 ka BP: Wei and Song 1992).

The climate of the study region is strongly influenced by the East Asian monsoon. In summer, monsoon rain penetrates the study region in early to mid-June, and retreats in September. In winter and



**Fig. 1** **A** Location of Dali Lake in China and major atmospheric circulation systems. EAWM is the East Asian winter monsoon and EASM is the East Asian summer monsoon. The blue dashed line indicates the modern position of the EASM limit. Numbers indicate sites referenced in the text: 1 Dali Lake, 2 Lake Xiarinur, 3 Lake Bayanchagan, 4 Lake Angulinur, 5 Sanbao Cave, 6 Dongge Cave. **B** Dali Lake and surrounding

region. The background is a digital elevation model (DEM, downloaded from <http://gdem.ersdac.jspacesystems.or.jp/index.jsp>, ASTER GDEM is a product of METI and NASA). The major inflowing rivers are: GR Gongger River, SR Salin River, LR Liangzi River, HR Haolai River. The white dashed line is the 1271 m a.s.l. contour of the DLW profile altitude

spring, the strong winter monsoon and westerly winds create favorable conditions for the development or intensification of cyclones and anticyclones, resulting in dust storms. Mean annual precipitation is 300–450 mm, with 70 % occurring from June–August. Mean annual evaporation is about 1287 mm (Compilatory Commission of Annals Banner 1993).

**Materials and methods**

**Lithology and sampling**

The Dali Lake West (DLW) profile (43°15′08.0″N, 116°26′41.3″E, 1271 m a.s.l.) (Fig. 2) and Dali Lake Southwest (DLSW) profile (43°10′12.93″N, 116°28′15.90″E, 1267 m a.s.l.) were excavated in exposed lake sediments in the western and southwestern part of the lake catchment, respectively. The sequence of the DLW profile (Fig. 2) consists of 223 cm of silty clays, silty sands and fine sands, overlain by 10 cm of eolian sands and underlain by

basalt. The DLSW profile consists of 220 cm of clays, silty clays and fine sands. The profiles were cut back by 20–60 cm to eliminate weathering effects and contamination and then sampled at 1-cm intervals. Samples were stored in sealed plastic bags prior to transport to the laboratory.

**Radiocarbon dating**

Plant macrofossils are scarce in the sequences and therefore organic matter and shells were used for AMS <sup>14</sup>C dating. Ten bulk samples of the DLW profile and one shell sample of the DLSW profile were measured in the Institute of Heavy Ion Physics School of Physics at Peking University in Beijing, China and Beta Analytic Inc. in Miami, USA, respectively. The organic samples were pretreated using the standard Acid–Alkali–Acid (AAA) method (Mook and Streurman 1983). Any plant rootlets were first removed prior to treating the samples with HCl and NaOH to eliminate carbonates and humic acid, respectively, followed by HCl treatment again to remove modern atmospheric CO<sub>2</sub>. The shell was pretreated with acid etches to eliminate any potential



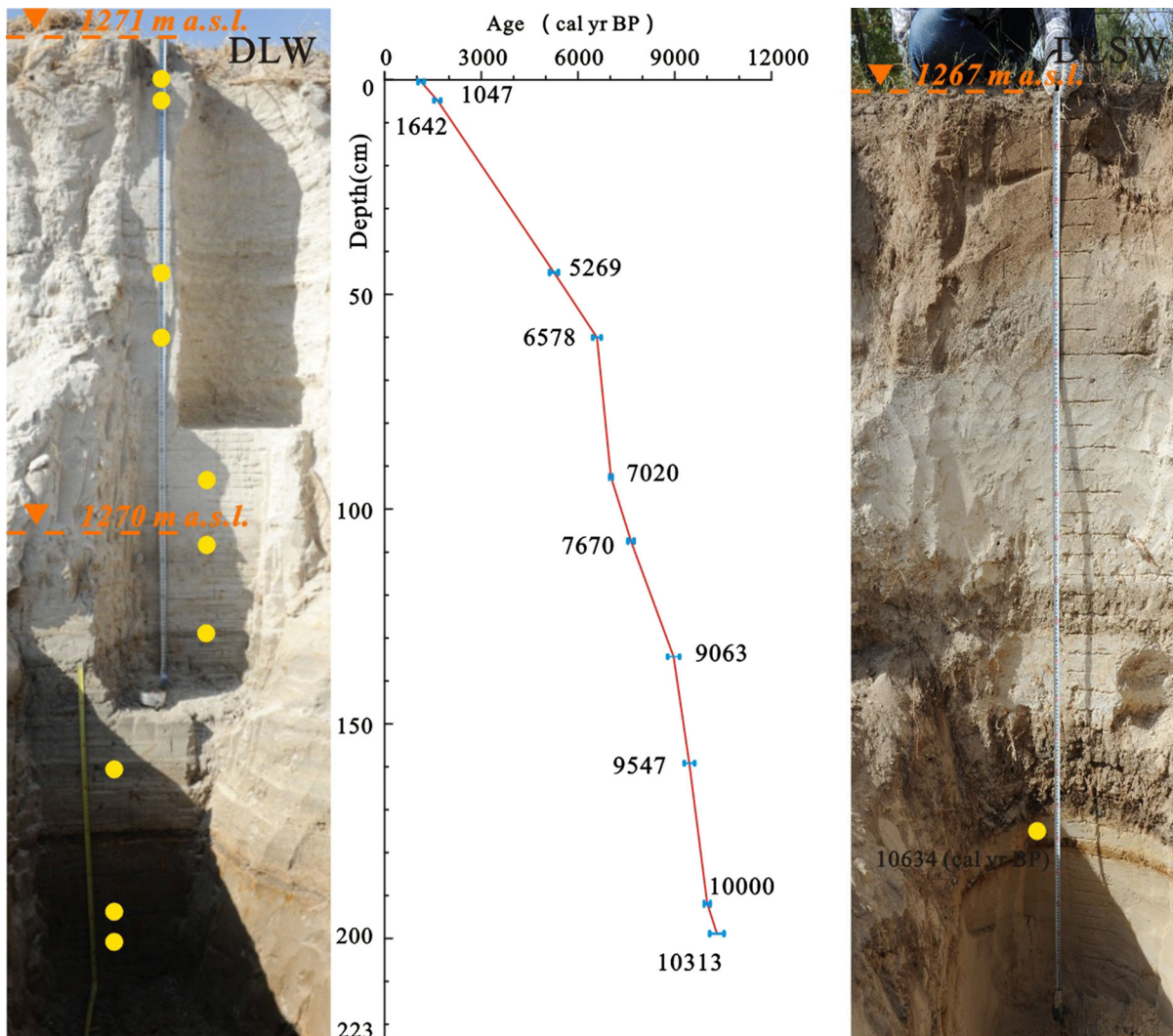


**Fig. 2** Photographs of the DLW and DLSW profiles with location of radiocarbon samples and age–depth curve for the DLW profile based on linear interpolation of the midpoint of the

age interval. The  $^{14}\text{C}$  ages are converted to cal year BP using OxCal 4.2 (Ramsey 2009) and reservoir-corrected (subtraction of 611 year)

secondary carbonate before radiocarbon dating. The residues were then combusted in a vacuum line and finally measured with the Accelerator Mass Spectrometry (AMS). All ages were calibrated to calendar years before present (cal year BP) using the Oxcal v 4.2 program (Ramsey 2009), with the IntCal 13 data set (Reimer et al. 2013) (Table 1).

#### Grain-size analysis

Pretreatment of the 443 sediment samples for grain-size analysis consisted of sequential removal

of organic matter and carbonates with 10–20 ml of 30 %  $\text{H}_2\text{O}_2$  and 10–15 ml 10 % HCl, respectively. Following HCl treatment, samples were rinsed at least three times with deionized water. Finally, the samples were dispersed by adding 10 ml of 0.05 M  $(\text{NaPO}_3)_6$  followed by treatment in an ultrasonic vibrator for 15 min. The grain-size distribution was measured using a Malvern Mastersizer 2000 laser grain-size analyzer with a measurement range of 0.02–2000  $\mu\text{m}$ . Each sample was analyzed twice, and the relative error was always <2 %.

**Table 1** Radiocarbon dates of samples from DLW and DLSW profiles

Sample ID	Laboratory number	Depth (cm)	Dating material	AMS <sup>14</sup> C age (year BP)	±Error (year)	Calibrated <sup>14</sup> C age (2σ) (cal year BP)
11DL-C1	BA111045	0.5	Organic matter	1750	30	1729–1565
12DL-GZ5	BA121127	5	Organic matter	2255	25	2344–2158
11DL-C2	BA111046	45	Organic matter	5145	45	5993–5750
12DL-GZ60	BA121128	60	Organic matter	6250	30	7260–7027
12DL-GZ93	BA121129	93	Organic matter	6785	40	7680–7579
12DL-GZ108	BA121130	108	Organic matter	7465	35	8366–8195
11DL-C3	BA111047	135	Organic matter	8720	35	9885–9551
12DL-GZ160	BA121131	160	Organic matter	8980	30	10,232–9940
12DL-GZ193	BA121133	193	Organic matter	9380	35	10,697–10,515
12DL-GZ200	BA121135	200	Organic matter	9570	50	11,125–10,724
15DLSW-167	Beta-390458	167	Shell	9870	40	11,385–11,207

### Partitioning of grain-size components

The grain size-standard deviation method was used to distinguish different grain-size components. The original data from grain-size measurement results were exported with the range from  $\log_2(-2)$  to  $\log_2 10$  with 0.1 intervals, and got 103 grain-size fractions. Then the standard deviations of the 103 fractions were calculated. The standard deviation is a measure of the dispersion of the data, with high values indicating significant non-homogeneity (Ma et al. 2013). A grain-size fraction with a high standard deviation can thus be regarded as the modal grain-size of an environmentally sensitive component (Sun et al. 2003). The component between two neighboring low standard deviations is considered to be sensitive to a particular environment and depositional process.

## Results

### Chronology

In paleo-limnologic studies, calibrated <sup>14</sup>C dates are often older than the true sediment ages. This may be due to the presence of reworked older organic material in the sediment core or to the well-documented hard water effect (Oldfield et al. 1997; Xiao et al. 2008; Chu et al. 2014). In this study, we corrected the sediment ages using a carbon reservoir age of 611 years, which

was surface intercept based on age–depth model by third-order polynomial fit in a previous study of Dali Lake (Xiao et al. 2008). The sampling positions and age-depth relationship by linear interpolation are shown in Fig. 2. The development of lake sediments at the bottom may correspond to the early Holocene.

### Analysis of the grain-size components

Figure 3 illustrates representative grain-size frequency distribution plots for the samples. Most of the samples in the DLW profile exhibit four well-defined peaks and five troughs, and in the DLSW profile there are three peaks and four troughs. The results of standard deviations for the 103 grain-size fractions are shown in Fig. 4a. Four grain-size ranges with high standard deviations exist in the DLW samples, centered on 1.03, 10, 104 and 478  $\mu\text{m}$ , which can be used to define components with the following corresponding grain-size ranges: C1 <1.07  $\mu\text{m}$ ; C2 1.07–39  $\mu\text{m}$ ; C3 39–256  $\mu\text{m}$ ; C4 >256  $\mu\text{m}$ . Three grain-size ranges with high standard deviations exist in the DLSW samples, centered on 1.03, 20 and 148  $\mu\text{m}$ , which made the components to be: C1 <1.07  $\mu\text{m}$ ; C2 1.07–60  $\mu\text{m}$ ; C3 >60  $\mu\text{m}$ . The small differences between two profiles reflect the different hydrodynamic force in different parts of lake. The frequency of occurrence of maxima in the different grain-size fractions (Fig. 4b) demonstrate that the grain size with the highest content in each sample is centered on 1, 9, 84 and 550  $\mu\text{m}$  in the

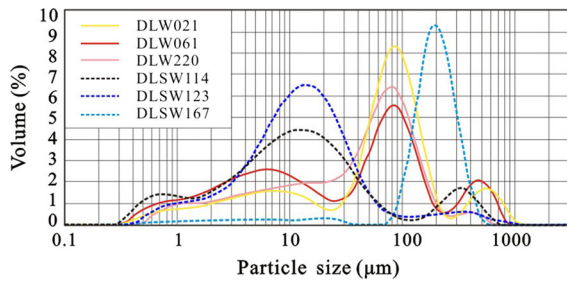


**Fig. 3** Representative grain-size frequency distribution curves for samples from different depths of the profiles

DLW profile and on 1, 20 and 338  $\mu\text{m}$  in the DLSW profile, which are consistent with the components defined above, based on standard deviations. Therefore, we concluded that these components could be used to represent the most important grain-size characteristics of the profiles.

Consideration of the transport and depositional processes represented by the partitioned components may help characterize changes in sedimentary environment and thus enable reconstruction of hydrological changes in the lake and catchment. Variation trends of the components indicate good correlations with lithology (Fig. 5). Pearson's correlation coefficient

R was calculated by SPSS (Statistical Product and Service Solutions) version 16 for Windows (SPSS Inc., Chicago, Illinois) (Howitt and Cramer 2008) at the 0.01 significance level, using a 2-tailed test. A correlation matrix (Table 2) for the four components in the DLW profile produced the following R-values: 0.73 for C1 and C2;  $-0.67$  for C1 and C3; and  $-0.81$  for C2 and C3. For the three components in the DLSW profile, they are: 0.72 for C1 and C2;  $-0.75$  for C1 and C3; and  $-0.99$  for C2 and C3. Thus C1 and C2 are positively correlated and both C1 and C2 are negatively correlated with C3. However, C4 of the DLW profile is weakly correlated with the other components. Based on these results it is possible to speculate that the sediment transport and depositional processes reflected by C1 and C2 are identical and that they have an inverse relationship with those reflected by C3. The hydrodynamic conditions reflected by C4 are not related to those reflected by the other components.

Individual components can be recognized based on their modal peak and grain-size range (Sun et al. 2002; An et al. 2012; Ma et al. 2013). Typical lacustrine sediments in Daihai Lake (located close to Dali Lake) exhibit two peaks at  $<1$  and  $10 \mu\text{m}$  (Sun et al. 2001),

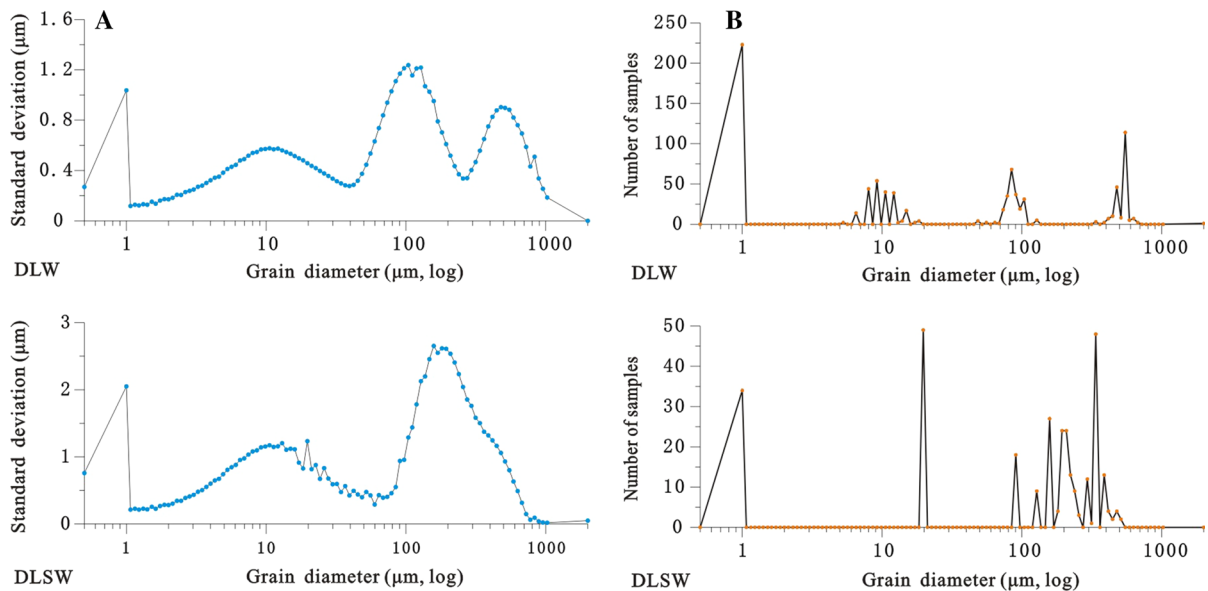


**Fig. 4** **A** Plots of the standard deviation of the 103 grain-size fractions. The maxima in standard deviation are interpreted as representing the modal values of the most environmentally-sensitive fractions. **B** Frequency of occurrence of maxima in

different grain-size fractions within the samples in the profiles. The results support the definition of the environmentally-sensitive fractions shown in plot (A)

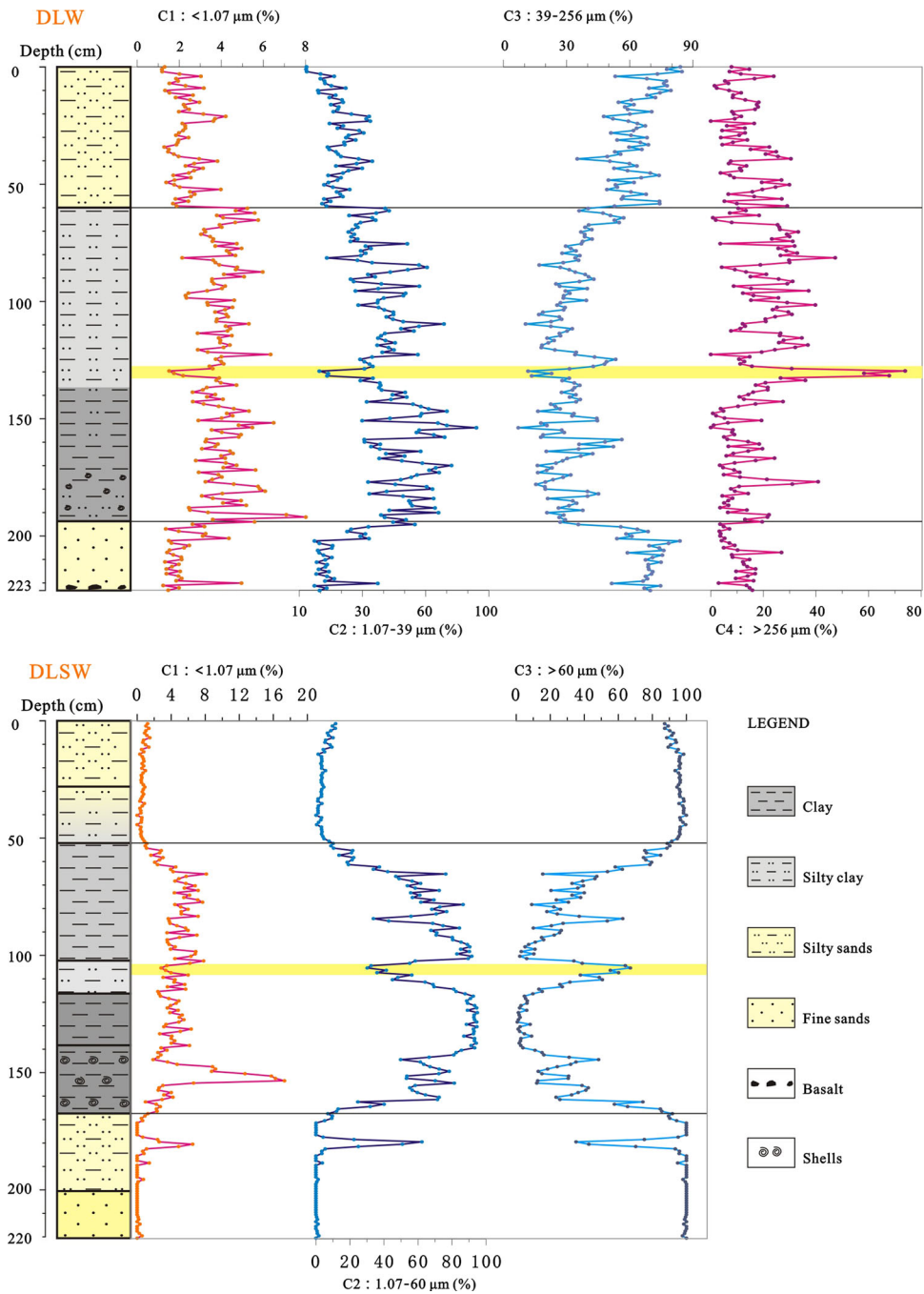


**Fig. 5** Depth series of the representation of the components defined in Fig. 4

consistent with components C1 and C2 of the samples, representing a low energy environment and a high water level. Therefore, C1 and C2 may be interpreted to represent long-term suspension and offshore suspension components. Since C3 is inversely correlated

with C1 and C2, it can be interpreted as representing a high-energy hydrodynamic environment and a low lake level, and is thus a nearshore suspension component. C4 component probably has not been significantly affected by hydrodynamic processes and only

been transported a short distance. The grain size of eolian sands, paleo-eolian sands and paleosols in the Otindag sandy land, South of Dali Lake is generally between 50 and 500  $\mu\text{m}$  (Liu et al. 2006), and thus such sources may contribute to the C4 component since its modal size is 478  $\mu\text{m}$  in the DLW profile. It is possible that it is wind-transported since the wind speed at Dali Lake may exceed  $17.2 \text{ m s}^{-1}$  (from Hexigten Meteorological Bureau). In addition, it is also possible that the C4 component could accumulate on the frozen lake surface in winter, and then be deposited on the lake bottom in spring after the ice has melted. Hydrodynamic forces within the lake would probably be too weak to alter the grain-size distribution of the C4 component and therefore it can be disregarded as a source of information about dynamical changes within the lake.

## Discussion

### Comparison with surface sediments

The key spatial characteristics of the grain-size of lake sediments are that it is uniform in a direction parallel to the shoreline but changes progressively from coarse to fine from the shore towards the center. Grain-size frequency distribution curves of surface sediment

samples in nearshore, transitional zone and offshore regions of present Dali Lake (Xiao et al. 2015) exhibit four and three modal values respectively (Fig. 6), which is similar to the sediments from the DLW and DLSW profiles. The samples of DLSW exhibit more offshore character because of relatively low elevation of the profile. Xiao et al. (2015) used a lognormal distribution function method to define five sedimentary components: long-term suspension (C'1), offshore suspension (C'2 and C'3), nearshore suspension (C'4) and nearshore saltation (C'5). Both C'2 and C'3 represent the same sedimentary dynamics, and the mode of C'2 is  $<0.3 \%$ . The C1–C4 components of the DLW sediments, partitioned by the grain-size standard deviation method, represent long-term suspension, offshore suspension, nearshore suspension and nearshore saltation components, respectively. The C2 component corresponds to the C'2 + C'3 components of Xiao et al. (2015); C3 corresponds to C'4; and C4 corresponds to C'5. Therefore, we conclude that the components partitioned by the two methods are comparable.

The surface sediment samples (Fig. 6) are from nearshore, transitional and offshore zones with depths of ca. 2 m (a3), 6 m (a7) and  $>8$  m (a11), respectively. Sediments in the offshore zone have four components (C'1–C'4) and lack the coarse component, C'5. In the transitional and nearshore zones the sediments are

**Table 2** Pearson correlation matrix of each component

			C1	C2	C3	C4
DLW profile	C1	Correlation coefficient	1			
		Significance test P (2-tailed)				
	C2	Correlation coefficient	0.729**	1		
		Significance test P (2-tailed)	0.000			
	C3	Correlation coefficient	−0.670**	−0.812**	1	
		Significance test P (2-tailed)	0.000	0.000		
	C4	Correlation coefficient	−0.095	−0.238	−0.372	1
		Significance test P (2-tailed)	0.159	0.000	0.000	
DLSW profile	C1	Correlation coefficient	1			
		Significance test P (2-tailed)				
	C2	Correlation coefficient	0.72**	1		
		Significance test P (2-tailed)	0.000			
	C3	Correlation coefficient	−0.75**	0.99**	1	
		Significance test P (2-tailed)	0.000	0.000		

\*\* Represents significant correlations at the 0.01 level (2-tailed)



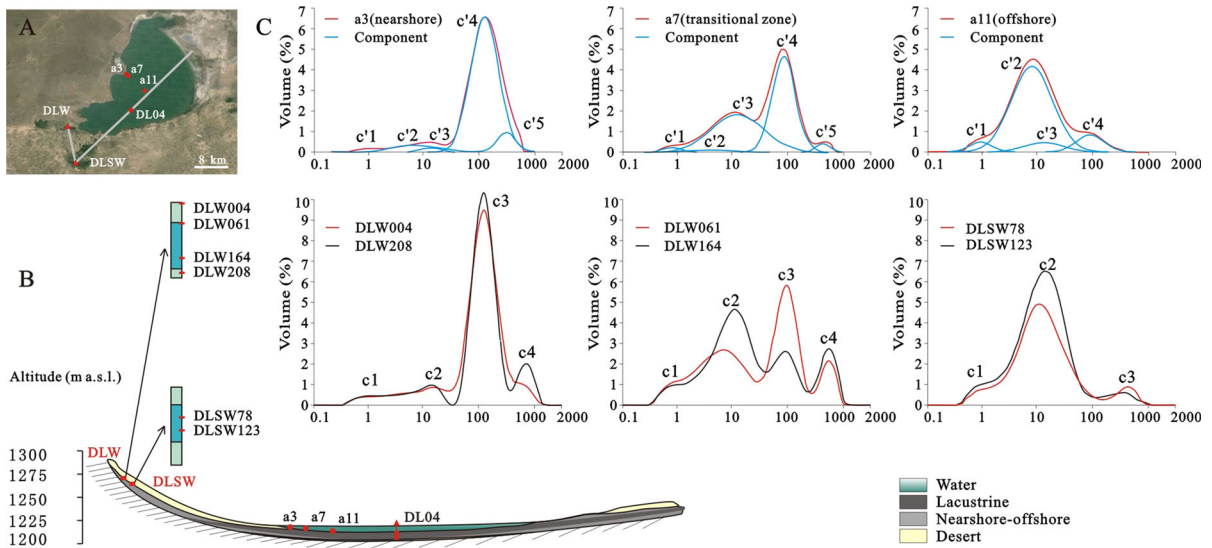


**Fig. 6** **A** Location of the DLW and DLSW sections, deep-water sediment core DL04 (Xiao et al. 2008; 2009) and the modern surface sediment samples *a3* (nearshore zone), *a7* (transitional zone) and *a11* (offshore zone) analyzed by Xiao et al. (2015). **B** Schematic section across the Dali Lake basin showing the relative locations of the profiles (with the position of the samples shown in c, modern surface sediment samples *a3* and *a7*, and deep-water core DL04). **C** Comparison of the grain-size frequency distribution curves of samples from the DLW and DLSW sections with modern surface sediment samples. The

frequency distribution curves for samples DLW004 and DLW208 from the upper and lower parts of the DLW section are consistent with the modern surface sediment sample from the nearshore zone; and the curves for samples DLW061 and DLW164 from the middle part of the DLW section are consistent with the modern surface sediment samples from the transitional zone; DLSW78 and DLSW123 from the middle part of the DLSW section are consistent with the modern surface sediment samples in the offshore zone

composed of five components (C'1–C'5). The representation of the long-term suspension (C'1) and offshore suspension (C'2 and C'3) components is <1 %, while that of the nearshore suspension component (C'4) is almost 7 % in the nearshore zone. In the transitional zone the representation of the long-term suspension components increased to about 1 %, and that of the offshore suspension component increased to about 2 %, while nearshore suspension component decreased to about 5 % (Fig. 6). The contribution variations of the long-term suspension, offshore suspension and nearshore suspension in the DLW and DLSW samples that vary in accordance with the lithology of the sections (Fig. 5) indicate the past occurrence of offshore, nearshore and transitional depositional environments at the location of the profiles.

### History of lake-level changes

The grain-size distribution in the sections of the sediment profiles interpreted to represent the near-

shore and transitional environments of the palaeolake resemble sediment samples in the modern lake taken at 2–8 m water depth. We therefore assume that the water table was only slightly above the elevation of the sediment profiles during the deposition of the DLW and DLSW sections. In Fig. 7 we provide a scenario of lake-level changes at Dali Lake, which is in agreement with these assumptions. The record can be divided into the following four stages: (1) from early Holocene to 10.0 cal ka BP; the lithology consists of fine sands. The mode of the C3 component is over 8 %, and that of the C1 and C2 components is less than 1 %, indicating that both profiles were located in the nearshore zone with a water depth that may have been around 2 m. (2) 10.0–6.6 cal ka BP; the lithology consists of silty clay and fine sands with occasional mollusk shells at the base. The mode of the C1 and C2 components in both profiles increased significantly compared to the previous stage, while C3 decreased dramatically, indicating an interval of high lake level with a water depth, which may have been around 6 m. (3) 6.6–1.0 cal ka BP; the lithology consists mainly of

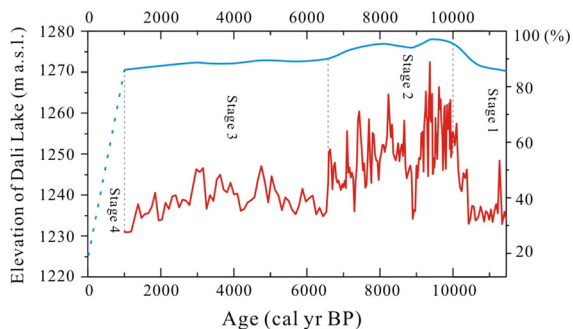


**Fig. 7** Time series of the proportional representation of grain-size component C2 (*red line*) from the DLW section. The *blue line* shows a scenario for changes in lake-level elevation of Dali Lake. The trends of the two records are consistent. (Color figure online)

silty sands and fine sands. The mode of the C1 and C2 components falls below 1 % and that of the near shore suspension component rises to over 8 %, indicating a significant reduction of lake level to a depth which may have been around 2 m. (4) After 1.0 cal ka BP, the accumulation of lacustrine sediments terminated at the DLW site, followed by the accumulation of eolian sands. Thus the lake was in a low level stage. The lacustrine record comes from 1271 m a.s.l. illustrate the lake have been above 1271 m a.s.l. for much of the Holocene, which was at least 45 m above the present altitude (modern observation 1226 m a.s.l.).

Based on the down-profile variation of the component frequency curves, a prominent climatic event can be identified at a depth of 132–130 cm in the DLW and 102–108 cm in the DLSW (indicated by yellow shading in Fig. 5). Compared to the average values during the ca. 1000 years preceding this event, for the DLW profile the long-term suspension (C1), offshore suspension (C2) and nearshore suspension (C3) components decreased from 3.9, 44.4 and 29.8 % to 1.85, 15.5 and 16 % respectively, implying a drastically decreased lake level and thus a dry climatic event. The nearshore saltation component (C4) increased from 21.9 to 66.7 %, also indicating a strong eolian activity. This event is dated to ca. 8.8 cal ka BP based on linear interpolation between the dated horizons. However, the climate event is not clearly evident in the record of the sediment core from the center of Dali Lake, thus demonstrating the potentially increased environmental sensitivity of the nearshore sediment record.

Although the grain-size and biomagnetic records from the lake center (Xiao et al. 2009; Liu et al. 2015)

(Fig. 8) showed great consistency with more detailed information than the nearshore profiles, the later could give us more evidences of paleo-lake level and specific climate event. Therefore, it is of great importance to combine the records from the deepwater and nearshore region to investigate the paleo-lake history. The similarity between the two shallow water sections indicates the nearshore profile will be suitable for study as long as they are far towards the shore or center of the lake, to ensure the continuity and sensitivity of the deposition.

The overall consistency between the results from the nearshore sections and the deep-water sediment core indicates that the former does not contain major hiatuses. Combining the results from the profiles and the deep-water core, it can be concluded that Dali Lake experienced the sequence of medium–high–medium–low level stages during the Holocene. From early Holocene to 10.0/9.8 cal ka BP, the lake was in a medium level stage, which was succeeded by a rapid change to a high level phase until 7.1/6.6/5.9 cal ka BP. The level then decreased to a medium stage with a slight rising tendency, until 1.8/1.0 cal ka BP. After 1.8/1.0 cal ka BP, the lake level declined further and was in a low level stage.

Lake Xiarinur, in the central area of the Otindag Sandy Land, also exhibits a rapid lake-level increase between 11.7 and 10.2 cal ka BP (Tang et al. 2015). The most humid period at Lake Bayanchagan, which is about 200 km southwest of Dali Lake, occurred between ~10.5 and ~6.5 cal ka BP (Jiang et al. 2006; 2010). In Lake Angulinur, wet and warm conditions occurred from ~10.9 to 7.4 cal ka BP (Wang et al. 2010). The East Asian Summer Monsoon (EASM) intensity as recorded by the stalagmite  $\delta^{18}\text{O}$  from Sanbao Cave (Dong et al. 2010) and Dongge Cave (Dykoski et al. 2005) declined dramatically at ~11.5 ka BP (corrected using an initial  $^{230}\text{Th}/^{232}\text{Th}$  date) and remained low from ~6.5 to 6 ka BP (date also corrected). This regional accordence indicates that the lake-level evolution was a response to the variation of the EASM, which was intensified by increased Northern Hemisphere summer insolation (Berger and Loutre 1991) during the Holocene climatic optimum. With regard to the dramatic decline of lake level since 1.0 cal ka BP, in addition to a weakened EASM, a recent study indicates that headward erosion and groundwater sapping by the Xilamulun River (Yang et al. 2015) would also have

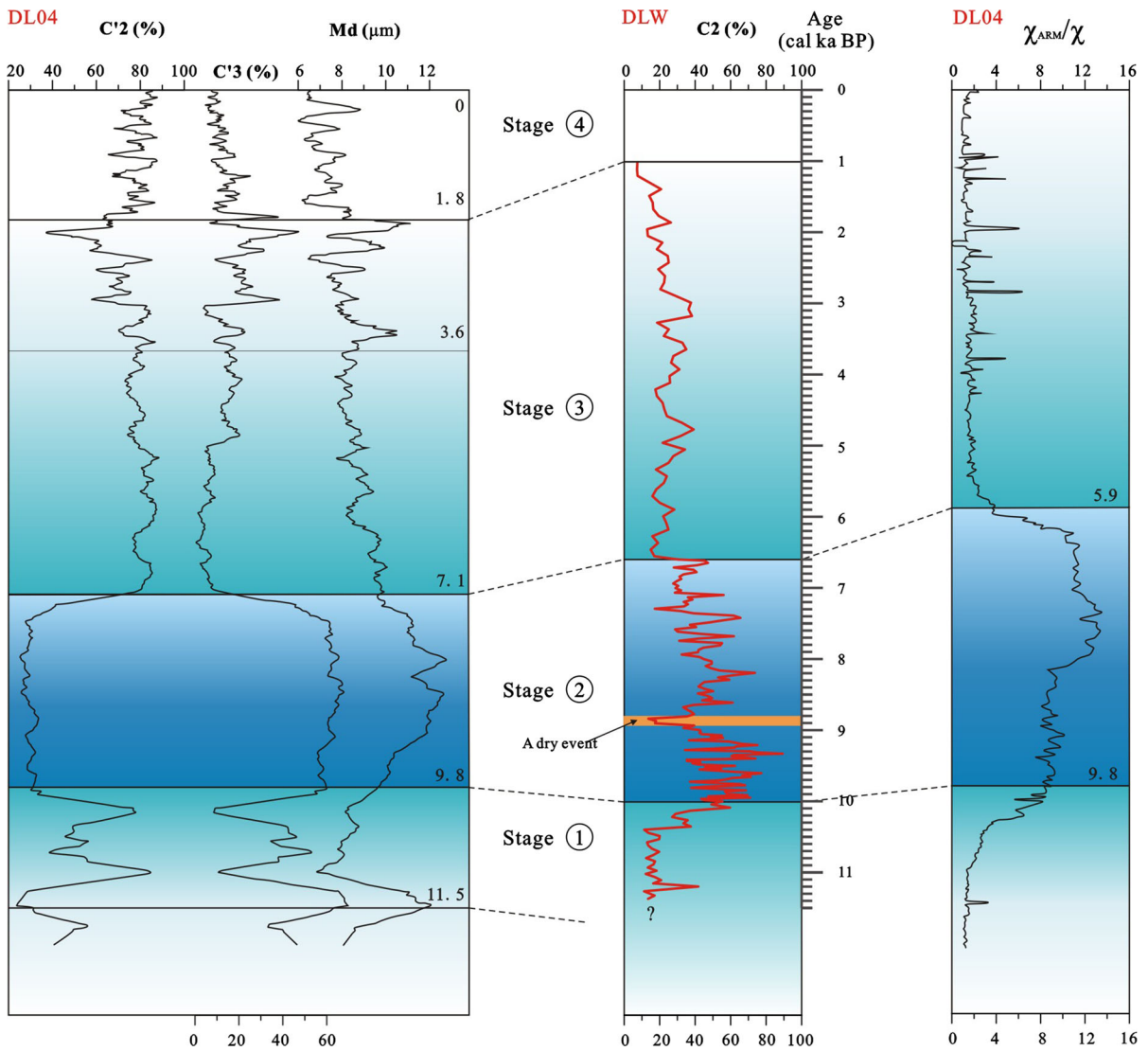


**Fig. 8** Comparison of the time series of two grain-size components, the median grain size (Xiao et al. 2009) and magnetic grain size (with revised age model, Liu et al. 2015) of deep-water core DL04 from Dali Lake with the time series of grain-size component C2 from the DLW section. Stages 1–3

refer to the lake-level stages referred to in the main text. Note that the inferred lake-level decrease (a dry event; orange shading) is much more clearly recorded in the DLW section than in the deep-water core

contributed significantly to the fall in lake level. Strong tectonic activity in late Holocene (2 ka BP; Wei and Song 1992) may also play an important role in this huge drop.

**Conclusions**

1. We have used a grain-size standard deviation method to partition the components of grain-size

records from marginal sediments from Dali Lake, North China, and compared the results with those from modern surface sediments collected from various depths, and with those from a deep-water core from the same site. The down-profile variation in the contribution of the various components, combined with the results of <sup>14</sup>C dating, can be used to construct a record of lake-level change at the site.

2. The following sequence of lake-level stages is inferred: (1) A medium lake-level stage from

early Holocene to 10.0 cal ka BP; (2) a high lake-level stage from 10.0 to 6.6 cal ka BP; (3) a return to a medium lake-level stage from 6.6 to 1.0 cal ka BP; and (4) a low lake-level stage after 1.0 cal ka BP.

3. The lake-level change history is broadly consistent with that obtained from an open-water sediment core from Dali Lake. However, a significant climatic event recorded in the lake margin profile is not recorded in the deep-water core. Thus the marginal sediments exhibit potentially greater environmental sensitivity.
4. The evolution of Dali Lake is generally consistent with that of other lakes in the region and with speleothem  $\delta^{18}\text{O}$  records from southern and central China, which are sensitive to variations in the intensity of the EASM controlled by changing summer insolation over the Northern Hemisphere.

**Acknowledgments** We thank Oliver Heiri and three anonymous referees for valuable comments and suggestions that helped improve the early version of the manuscript. Special thanks are extended to Thomas J Whitmore and Oliver Heiri for their careful revision of the manuscript. This study was financially supported by the Grants from the Geological Investigation Projects of China Geological Survey (Nos. 12120113005600, 1212011120142, 121201102000150010-07).

## References

- An FY, Ma HZ, Wei HC, Lai ZP (2012) Distinguishing aeolian signature from lacustrine sediments of the Qaidam Basin in northeastern Qinghai-Tibetan Plateau and its palaeoclimatic implications. *Aeolian Res* 4:17–30
- Ashley GM (1978) Interpretation of polymodal sediments. *J Geol* 86:411–421
- Bacon SN, Burke RM, Pezzopane SK, Jayko AS (2006) Last glacial maximum and Holocene lake levels of Owens Lake, eastern California, USA. *Quat Sci Rev* 25:1264–1282
- Benson LV, Smoot JP, Lund SP, Mensing SA, Foit FF, Rye RO (2013) Insights from a synthesis of old and new climate-proxy data from the Pyramid and Winnemucca lake basins for the period 48 to 11.5 cal ka. *Quat Int* 310:62–82
- Berger A, Loutre M (1991) Insolation values for the climate of the last 10 million years. *Quat Sci Rev* 10:297–317
- Boulay S, Colin C, Trentesaux A, Pluquet F, Bertaux J, Blamart D, Buehring C, Wang P (2003) Mineralogy and sedimentology of Pleistocene sediment in South China Sea. *Proc ODP Sci Results* 184:1–21
- Campbell C (1998) Late Holocene lake sedimentology and climate change in southern Alberta, Canada. *Quat Res* 49:96–101
- Chu GQ, Sun Q, Xie MM, Lin Y, Shang WY, Zhu QZ, Shan YB, Xu DK, Rioual P, Wang L, Liu JQ (2014) Holocene cyclic climatic variations and the role of the Pacific Ocean as recorded in varved sediments from northeastern China. *Quat Sci Rev* 102:85–95
- Cohen AS (2003) *Paleolimnology: the history and evolution of lake systems*. Oxford University Press, New York **528 pp**
- Compilatory Commission of Annals Banner (1993) *Annals of Hexigten Banner*. People's Press of Inner Mongolia, Hohhot, pp 97–106 (in Chinese)
- Dong JG, Wang YJ, Cheng H, Hardt B, Edwards RL, Kong XG, Wu JY, Chen ST, Liu DB, Jiang XY (2010) A high-resolution stalagmite record of the Holocene East Asian monsoon from Mt Shennongjia, central China. *The Holocene* 20:257–264
- Dykoski CA, Edwards RL, Cheng H, Yuan DX, Cai YJ, Zhang ML, Lin YS, Qing J, An ZS, Revenaugh J (2005) A high-resolution, absolute-dated Holocene and deglacial Asian monsoon record from Dongge Cave, China. *Earth Planet Sci Lett* 233:71–86
- Folk RL, Ward WC (1957) Brazos River bar: a study in the significance of grain size parameters. *J Sediment Petrol* 27:3–26
- Geng K, Zhang ZC (1988) The geomorphic characteristics and evolution of the lakes in Dalairuoeer area of Neimenggu Plateau during the Holocene. *J Beijing Norm Univ (Nat Sci Ed)* 4:94–101 (in Chinese)
- Håkanson L, Jansson M (1983) *Principles of lake sedimentology*. Springer, Berlin **316 pp**
- Howitt D, Cramer D (2008) *Introduction to SPSS in psychology: for version 16 and earlier*. Pearson Education, Harlow **377 pp**
- Jiang WY, Guo ZT, Sun XJ, Wu HB, Chu GQ, Yuan BY, Hatté C, Guiot J (2006) Reconstruction of climate and vegetation changes of Lake Bayanchagan (Inner Mongolia): holocene variability of the East Asian monsoon. *Quat Res* 65:411–420
- Jiang WY, Guiot J, Chu GQ, Wu HB, Yuan BY, Hatté C, Guo ZT (2010) An improved methodology of the modern analogues technique for palaeoclimate reconstruction in arid and semi-arid regions. *Boreas* 39:145–153
- Krumbein WC (1938) Size frequency distributions of sediments and the normal phi curve. *J Sediment Res* 8:84–90
- Li RQ, Zheng LM, Zhu GR (1990) Lakes and environmental changes in Inner Mongolia Plateau. Beijing Normal University Press, Beijing, pp 45 (in Chinese)
- Liu SL, Wang T, Guo J (2006) Characteristics of blown sand activities in Hunshandake Sandy Land in spring. *J Desert Res* 26:356–361 (in Chinese)
- Liu XQ, Dong HL, Yang XD, Herzs Schuh U, Zhang EL, Stuet JW, Wang YB (2009) Late Holocene forcing of the Asian winter and summer monsoon as evidenced by proxy records from the northern Qinghai-Tibetan Plateau. *Earth Planet Sci Lett* 280:276–284
- Liu SZ, Deng CL, Xiao JL, Li JH, Paterson GA, Chang L, Yi L, Qin HF, Pan YX, Zhu RX (2015) Insolation driven bi-magnetic response to the Holocene Warm Period in semi-arid East Asia. *Sci Rep* 5:8001
- Ma L, Wu JL, Wen JH, Liu W, Jilili A (2013) Grain size characteristics and its environmental significance of



- lacustrine sediment recorded in Wuliangsu Lake, Inner Mongolia. *Acta Sedimentol Sin* 31:646–652 (in Chinese)
- Middleton GV (1976) Hydraulic interpretation of sand size distributions. *J Geol* 84:405–426
- Mook WG, Streurman HJ (1983) Physical and chemical aspects of radiocarbon dating. In: Proceedings of the first international symposium 14 C and archaeology. Council of Europe, Groningen, 1981, pp 31–55
- Negrini RM, Wigand PE, Draucker S, Gobalet K, Gardner JK, Sutton MQ, Yohe RM II (2006) The Rambla highstand shoreline and the Holocene lake-level history of Tulare Lake, California, USA. *Quat Sci Rev* 25:1599–1618
- Nishizawa S, Currey DR, Brunelle A, Sack D (2013) Bonneville basin shoreline records of large lake intervals during Marine Isotope Stage 3 and the Last Glacial Maximum. *Palaeogeogr Palaeoclimatol Palaeoecol* 386:374–391
- Oldfield F, Crooks PRJ, Harkness DD, Petterson G (1997) AMS radiocarbon dating of organic fractions from varved lake sediments: an empirical test of reliability. *J Paleolimnol* 18:87–91
- Peng YJ, Xiao JL, Nakamura T, Liu BL, Inouchi Y (2005) Holocene East Asian monsoonal precipitation pattern revealed by grain-size distribution of core sediments of Daihai Lake in Inner Mongolia of north-central China. *Earth Planet Sci Lett* 233:467–479
- Qin XG, Cai BG, Liu TS (2005) Loess record of the aerodynamic environment in the east Asia monsoon area since 60,000 years before present. *J Geophys Res* 110:B01204. doi:10.1029/2004JB003131
- Ramsey CB (2009) Bayesian analysis of radiocarbon dates. *Radiocarbon* 51:337–360
- Reheis MC, Bright J, Lund SP, Miller DM, Skipp G, Fleck RJ (2012) A half-million-year record of paleoclimate from the Lake Manix core, Mojave Desert, California. *Palaeogeogr Palaeoclimatol Palaeoecol* 365–366:11–37
- Reheis MC, Adams KD, Oviatt CG, Bacon SN (2014) Pluvial lakes in the Great Basin of the western United States—a view from the outcrop. *Quat Sci Rev* 97:33–57
- Reimer PJ, Bard E, Bayliss A, Beck JW, Blackwell PG, Ramsey CB, Buck CE, Cheng H, Edwards RL, Friedrich M (2013) IntCal13 and Marine13 radiocarbon age calibration curves 0–50,000 years cal BP. *Radiocarbon* 55:1869–1887
- Sun QL, Zhou J, Xiao JL (2001) Grain-size characteristics of Lake Daihai sediments and its paleoenvironment significance. *Mar Geol Quat Geol* 21:93–95 (in Chinese)
- Sun DH, Bloemendal J, Rea DK, Vandenberghe J, Jiang FC, An ZS, Su RX (2002) Grain-size distribution function of polymodal sediments in hydraulic and aeolian environments, and numerical partitioning of the sedimentary components. *Sediment Geol* 152:263–277
- Sun YB, Gao S, Li J (2003) Preliminary analysis on sensitive grain size component of terrigenous material from marginal sea. *Chin Sci Bull* 48:83–86 (in Chinese)
- Tang L, Wang XS, Zhang SQ, Chu GQ, Chen Y, Pei JL, Sheng M, Yang ZY (2015) High-resolution magnetic and palynological records of the last deglaciation and Holocene from Lake Xiarinur in the Hunshandake Sandy Land, Inner Mongolia. The Holocene. doi:10.1177/0959683615571426
- Visher SG (1969) Grain-size distribution and depositional processes. *J Sediment Res* 39:1074–1106
- Wang HY, Liu HY, Zhu JL, Yin Y (2010) Holocene environmental changes as recorded by mineral magnetism of sediments from Anguli-nuur Lake, southeastern Inner Mongolia Plateau, China. *Palaeogeogr Palaeoclimatol Palaeoecol* 285:30–49
- Wang JZ, Wu JL, Zeng HA (2014) Grain size characteristics and its environmental significance of Lake Chengpuhai sediments in Hetao Plain, Inner Mongolia. *Mar Geol Quat Geol* 34:137–144 (in Chinese)
- Wei YM, Song CQ (1992) Neotectonic movement and lake evolution in Palaeo-Jingpeng Lake area, Inner-Mongolia. *Arid Land Geography* 15:34–41 (in Chinese)
- Weltje GJ (1997) End-member modeling of compositional data: numerical-statistical algorithms for solving the explicit mixing problem. *Math Geol* 29:504–549
- Wen RL, Xiao JL, Chang ZG, Zhai DY, Xu QH, Li YC, Itoh S, Lomtatidze Z (2010) Holocene climate changes in the mid-high-latitude-monsoon margin reflected by the pollen record from Hulun Lake, northeastern Inner Mongolia. *Quat Res* 73:293–303
- Xiao JL, Xu QH, Nakamura T, Yang XL, Liang WD, Inouchi Y (2004) Holocene vegetation variation in the Daihai Lake region of north-central China: a direct indication of the Asian monsoon climatic history. *Quat Sci Rev* 23:1669–1679
- Xiao JL, Si B, Zhai DY, Itoh S, Lomtatidze Z (2008) Hydrology of Dali Lake in central-eastern Inner Mongolia and Holocene East Asian monsoon variability. *J Paleolimnol* 40:519–528
- Xiao JL, Chang ZG, Si B, Qin XG, Itoh S, Lomtatidze Z (2009) Partitioning of the grain-size components of Dali Lake core sediments: evidence for lake-level changes during the Holocene. *J Paleolimnol* 42:249–260
- Xiao JL, Fan JW, Zhai DY, Wen RL, Qin XG (2015) Testing the model for linking grain-size composition to lake level status of modern clastic lakes. *Quat Int* 355:34–43
- Yang XP, Scuderi LA, Wang XL, Scuderi LJ, Zhang DG, Li HW, Forman S, Xu QH, Wang RC, Huang WW, Yang SX (2015) Groundwater sapping as the cause of irreversible desertification of Hunshandake Sandy Lands, Inner Mongolia, northern China. *Proc Natl Acad Sci* 112:702–706
- Zhang CJ, Zhang WY, Feng ZD, Mischke S, Gao X, Gao D, Sun FF (2012) Holocene hydrological and climatic change on the northern Mongolian Plateau based on multi-proxy records from Lake Gun Nuur. *Palaeogeogr Palaeoclimatol Palaeoecol* 323–325:75–86
- Zhen ZL, Zhang S, Shi XH, Sun B (2013) Research on the evolution of Dali Lake area based on the remote sensing technology. *China Rural Water Hydropower* 7:6–9 (in Chinese)
- Zhen ZL, Li CY, Li WB, Hu QT, Liu XX, Liu ZJ, Yu RX (2014) Characteristics of environmental isotopes of surface water and groundwater and their recharge relationships in Lake Dali basin. *J Lake Sci* 26:916–922 (in Chinese)